A UV-photofragmentation/laser-induced fluorescence sensor for the atmospheric detection of nitrous acid

ARTICLE *in* ENVIRONMENTAL SCIENCE AND TECHNOLOGY · SEPTEMBER 1989

Impact Factor: 5.33 · DOI: 10.1021/es00067a007

(20) Becker, W.; Schmale, H. *Comp. Biochem. Physiol.* **1978**, *59B*, 75-79.
(21) Trede, G.; Becker, W. *Comp. Biochem. Physiol.* **1982**, *73B*, 405-409.
(22) Becker, W. *Comp. Biochem. Physiol.* **1983**, *76B*, 215-219.
(23) Schnell, S.; Becker, W.; Winkler, A. *Comp. Biochem. Physiol.* **1985**, *81B*, 1001-1008.
(24) Wolmarans, C. T.; Mienie, L. J.; Strydom, D. *Comp. Biochem. Physiol.* **1986**, *84A*, 335-337.
(25) Wolmarans, C. T.; Farrell, Z. *Comp. Biochem. Physiol.* **1987**, *86A*, 773-776.
(26) Patience, R. L.; Thomas, J. D.; Sterry, P. R. *Comp. Biochem. Physiol.* **1983**, *76B*, 253-262.
(27) Wilson, R. A. *Comp. Biochem. Physiol.* **1968**, *24*, 629-633.
(28) Zylstra, U. *Neth. J. Zool.* **1972**, *22*, 283-298.
(29) Thomas, J. D.; Benjamin, M.; Lough, A.; Aram, R. H. *J. Anim. Ecol.* **1974**, *43*, 839-860.
(30) Denny, M. In *Mollusca*; Hochachka, P. W., Ed.; Academic Press: London, 1983; Vol. 1, pp 431-465.
(31) Lock, R. A. C.; Van Overbeeke, A. P. *Comp. Biochem. Physiol.* **1981**, *69C*, 67-73.
(32) Pärt, P.; Lock, R. A. C. *Comp. Biochem. Physiol.* **1983**, *76C*, 259-263.
(33) Cusimano, R. F.; Brakke, D. F.; Chapman, G. A. *Can. J. Fish. Aquat. Sci.* **1986**, *43*, 1497-1503.
(34) Thomas, J. D.; Tait, A. I. *Philos. Trans. R. Soc. London, B.* **1984**, *305*, 201-253.
(35) Thomas, J. D.; Ratcliffe, P. J. *Freshwater Biol.* **1973**, *3*, 573-612.

Received for review August 26, 1988. Accepted March 20, 1989. We thank the National Environment Research Council for financial support and Pilkington Controlled Release Systems for permission to publish this paper.

A UV-Photofragmentation/Laser-Induced Fluorescence Sensor for the Atmospheric Detection of HONO

Michael O. Rodgers* and Douglas D. Davis

School of Geophysical Sciences, Georgia Institute of Technology, Atlanta, Georgia 30332

■ An in situ laser-based detection system for measuring atmospheric HONO has been built and tested. This spectroscopic selective system has been tested for numerous chemical interferences. The results from these tests indicate that down to the tens of parts per trillion HONO concentration range no significant problems were detected. Sampling losses were also evaluated under varying atmospheric conditions and were found to be negligible at ambient levels of HONO amenable to controlled testing, e.g., the low ppbv range. The PF-LIF system as currently configured has a detection limit in the low tens of parts per trillion concentration range for typical integration times of 15 min in duration. This sensitivity is roughly equivalent to that achieved by the long-path differential absorption technique, but the PF-LIF has the added feature of being fully mobile and capable of in situ HONO measurements.

Introduction

Nitrous acid, HONO, has been postulated to be an important chemical intermediate in the chemistry of the troposphere (*1-4*). It appears to be of particular importance in urban areas where high concentrations of precursor species (i.e., NO/NO_2) result in significant HONO production (*5*). During daylight hours the production of HONO is very efficiently offset by its rapid photolysis, typically resulting in rather low steady-state concentrations of this species. At night, however, HONO loss rates are small and continual production leads to the accumulation of this species throughout the evening. In polluted air masses, for example, peak nighttime concentrations in the parts per billion (ppbv) range have been observed (*5, 6*).

To date, atmospheric HONO measuring techniques have either lacked spectroscopic selectivity, as when used in the in situ mode, or involved long-path optical detection methods that lead only to long-path integrated values of HONO. The nonspectroscopic techniques include a modification of a colorimetric technique for NO_2 detection (*7*) and a denuder tube technique (*8*). The former technique is now believed to be unreliable due to interference from other atmospheric nitrogen oxide species, i.e., PAN (*9*). In the denuder technique, a correction to the measurements is required to compensate for the effect of interfering HONO produced by reactions within the apparatus. The lack of significant diurnal variation in the HONO concentrations measured by this approach (*10*) also leaves questions as to whether these corrections can be made quantitatively.

Unequivocal measurements of HONO have been made using the technique of long-path optical differential absorption (*5, 6, 11-13*). However, as noted above, while this method provides spectroscopic identification of the HONO species, it suffers from significant performance degradation under conditions of poor visibility, such as fog or rain, and is not readily adapted to mobile sampling platforms, such as aircraft.

Here we report on the development of an in situ type detection system for atmospheric HONO that provides spectroscopic selectivity while retaining the advantages of the in situ detection approach. This instrument utilizes the technique of photofragmentation/laser-induced fluorescence, PF-LIF (*14*).

PF-LIF Detection of HONO. The optical absorption properties and photochemistry of HONO make it an excellent candidate for detection by the PF-LIF technique (*14-17*). HONO itself is nonfluorescent but has a near-ultraviolet absorption band involving a $\pi^* \leftarrow$ n type transition with a progression in the ν_2 stretch (*18*). Previous studies by investigators (*19, 20*) also have shown a near unity primary quantum yield (λ_1 = 365 nm) for the process

$$\mathrm{HONO} + h\nu_1 \rightarrow \mathrm{OH} + \mathrm{NO} \qquad (1)$$

In addition, both of the photofragments, OH and NO, may be readily detected by laser-induced fluorescence. Thus, the selection of the best PF-LIF detection scheme involves selecting the photofragment species that maximizes the achievable signal-to-noise ratio while avoiding interference from other atmospheric species.

Figure 1 shows the absorption spectrum of HONO along with that of NO_2 which, due to its higher atmospheric concentration relative to HONO, is considered to be the most likely photolytic interferent in the detection of the NO photofragment from HONO. By coincidence, the 354-nm HONO band lies in the vicinity of two of the most

 0013-936X/89/0923-1086$01.50/0

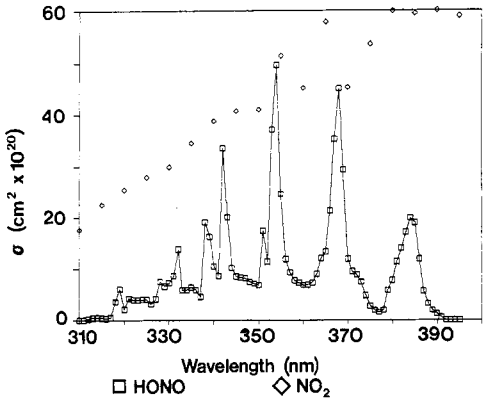

Figure 1. Comparison of NO_2 and HONO near-ultraviolet absorption cross sections (NASA 1983).

intense laser sources available in the near-ultraviolet spectral range, the third harmonic of Nd:YAG at 354.7 nm and the output wavelength of the XeF excimer laser at 353 nm. Thus, our originally proposed HONO detection scheme (*14*) used the Nd:YAG third harmonic to photofragment HONO as part of the detection sequence

$$\text{HONO} + h\nu_1(\lambda_1 = 355\text{ nm}) \rightarrow \text{OH(X)} + \text{NO(X, } v'' = 0, 1, 2) \quad (2)$$

$$\text{NO(X, } v'' = 2) + h\nu_2(\lambda_2 = 248\text{ nm}) \rightarrow \text{NO(A, } v' = 0) \quad (3)$$

$$\text{NO(A, } v' = 0) \rightarrow \text{NO(X, } v'' = 0) + h\nu_3(\lambda_3 = 226\text{ nm}) \quad (4)$$

Critical to this proposed PF–LIF scheme (*14*), however, is the assumption that at the photolysis wavelength of 355 nm, the photodecomposition of ambient NO_2 is not a significant source of the photofragment $NO(X^2\pi, v'' = 2)$. At first glance, this seems to be a reasonable assumption since production of $NO(X^2\pi, v'' = 2)$ from NO_2 requires the coupling of internal molecular energy into the photodecomposition process. However, recent observations (*21*) have shown that this assumption is invalid. At 355 nm, the latter study (*21*) determined that although the primary quantum yield for $v'' = 2$ NO production from photolysis of HONO exceeded that from NO_2 by a factor of ~7, the higher ambient concentration of NO_2 relative to HONO typically overwhelmed the higher NO $v'' = 2$ quantum yield from HONO. Thus, NO_2 represents a major interference to the NO PF–LIF detection scheme. The results from this investigation (*21*) also indicated that although finite in value the quantum yield for production of $NO(X^2\pi, v'' = 3)$ from the 355-nm photolysis of HONO was too small to make the detection of the $v'' = 3$ NO photofragment attractive.

As a result of these observations, the HONO detection scheme developed in this work was based on detection of the ground-state OH photofragment. [Note, that two independent studies have shown that vibrationally excited OH is not generated in the UV photolysis of HONO (*22*, *23*).]

The approach taken here thus involves the detection of ground-state OH using single-photon laser-induced fluorescence (SP–LIF) which, although not free of background fluorescence noise, is reasonably well established and has excellent sensitivity for OH detection at levels at or above 10^7 molecules/cm^3 (*16*). (Under our conditions for levels of HONO of 40 pptv, ~8×10^7 OH/cm^3 are produced.) The principal limitation of this approach is the well-documented interference resulting from the photolysis of atmospheric ozone by the 282-nm OH

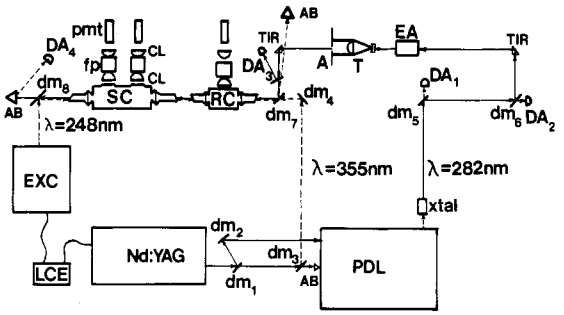

Figure 2. Optical layout for PF–LIF HONO detection system: A, aperture; AB, absorption beam dump; CL, fluorescence collection lens; DA, laser diode; DM, dichroic mirror; EA, laser energy attenuator; EXC, excimer laser; FP, optical filter pack; LCE, laser coupling electronics; PMT, photomultiplier tube; PDL, pulse dye laser; RC, reference cell; SC, sampling chamber; T, telescope; TIR, beam steering prism; XTAL, frequency doubling crystal.

analysis/probe laser beam. Ozone photolysis at this wavelength produces metastable atomic oxygen $O(^1D)$ that reacts rapidly with ambient water vapor to produce interferant OH radicals. Controlling this interference is an important element in the design and operation of any system using this approach and is discussed in detail in Appendix A. With the above considerations in mind, the PF–LIF HONO detection scheme finally used in this study is summarized as follows:

$$\text{HONO} + h\nu_1(\lambda_1 = 355\text{ nm}) \rightarrow \text{OH(X, } v'' = 0) + \text{NO(X)} \quad (5)$$

$$\text{OH(X, } v'' = 0) + h\nu_2(\lambda_2 = 282\text{ nm}) \rightarrow \text{OH(A, } v' = 1) \quad (6)$$

$$\text{OH(A, } v' = 1) + \text{M} \rightarrow \text{OH(A, } v' = 0) + \text{M}^* \quad (7)$$

$$\text{OH(A, } v' = 0, 1) \rightarrow \text{OH(X)} + h\nu_3(\lambda_3 \simeq 309\text{ nm}) \quad (8)$$

Experimental Hardware

General Description. The PF–LIF HONO system is composed of five major subsystems: (1) a Nd:YAG-driven dye laser system with its accompanying nonlinear crystals and beam-processing optics that produce the required photolysis and OH analysis/probe frequencies; (2) an air sampling system to collect outside air and deliver it to the sampling chamber; (3) a sampling chamber, equipped with the fluorescence collection optics and photomultiplier tube assemblies; (4) an electronic signal measurement system; and (5) a dynamic dilution type flow calibration system. Each of these subsystems is discussed in detail in the following text.

Lasers and Laser Optical Train. Figure 2 gives a schematic illustration of the optical layout used in the PF–LIF HONO detection system. Central to this system was a frequency-doubled and -tripled oscillator/amplifier Nd:YAG driven laser (Quanta Ray DCR IIa). The resulting second and third harmonic output wavelengths (at 532 and 355 nm, respectively) were separated from the Nd:YAG fundamental at 1.06 μ by a series of dichroic mirrors (DM_1–DM_4). Mirrors DM_1 and DM_2 served to separate out the 532-nm second harmonic, while mirrors DM_3 and DM_4 isolated the 355-nm third harmonic. After mirror DM_4, the energy of the 355-nm HONO photolysis beam was nominally 100 ± 10 mJ/pulse.

The 532-nm beam served as the optical pump for a Quanta Ray Model PDL-1a dye laser which, when using Rhodamine 590 dye in conjunction with an output frequency doubling crystal (KD*P), generated tunable 282-nm radiation for the detection of the OH photofragment. This system typically produced 2.5–3 mJ/pulse of tunable

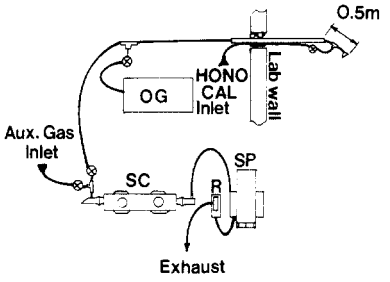

Figure 3. PF–LIF HONO air sampling system: OG, ozone generator; R, sample flow rotameter; SC, sampling pump.

UV radiation. Line scans of the frequency-doubled dye laser output (near 282 nm) over several isolated OH spectral lines resulted in an estimated effective linewidth for this system of 0.13 ± 0.03 cm^{-1}.

The frequency-doubled dye laser output was separated from the fundamental wavelength by using dichroic mirrors DM_5 and DM_6. Since the optical path between DM_5 and DM_6 was traversed only by the OH analysis/probe beam, variations in the effective pathlength could be used to adjust the relative time of arrival of the photolysis and OH analysis/probe beams at the sampling cell. For our experiments, the distance between DM_5 and DM_6 resulted in a delay in the arrival of the probe laser beam at the sampling region of ~14 ns, relative to the photolysis pulse. Since the width of both pulses was nearly half of the latter value (6–7 ns FWHM), the photolysis of HONO was over 90% complete before the arrival of the OH analysis/probe beam.

The UV steering prism located after DM_6 was used to steer the 282-nm beam through a variable optical attenuator that served to provide the desired input laser energy at the OH/HONO sampling cell. (Under typical measurement conditions approximately 0.2 mJ/pulse of 282-nm laser energy entered the sampling cell.) After adjustment of the UV laser energy, the beam was further processed by expansion in a 5× Galilean type telescope and then passed through a 1.0-cm aperture positioned ~5 cm behind the telescope. This optical processing sequence served both to create a more homogeneous 282-nm beam as well as to match the 282-nm beam diameter to that of the 355-nm photolysis beam. The enlarged beam had the dual advantage of reducing the 282-nm beam divergences and further reducing the O_3/H_2O interference problem (see Appendix A).

At mirror DM_7 the reflected 282-nm OH sampling beam was combined with the transmitted (T = 85–90%) 355-nm photolysis beam, and the combined beams were then directed through two optical cells. The first of these cells was used as a calibration/reference system, the second as the ambient air monitoring chamber.

The final mirror in the optical train, DM_8, served to direct the unpolarized output from a 248-nm KrF excimer laser (Quanta Ray Model EXC 401) into the HONO sampling chamber. This laser, denoted EXC in Figure 2, provided an independent means of calibrating the HONO system by generating an OH radical source from a well-characterized chemical gas mixture.

Air Sampling System. An important consideration in setting up the HONO ambient sample inlet line was guarding against the possible influence of surface reactions. Surface reactions could potentially cause a reduction in HONO levels due to surface decomposition or to system-generated artifacts due to surface-catalyzed HONO production. Recognizing these potential problems, the HONO sampling system, illustrated schematically in Figure 3, was constructed of materials (principally Teflon) that were found to be relatively inert to surface reactions involving HONO. In particular, no parts were used that would bring the sampled air stream in contact with metal surfaces. Details of the tests performed on this system to demonstrate the absence of system-generated artifacts are discussed later in the text under System Performance and are further elaborated on in the work by Rodgers (*17*).

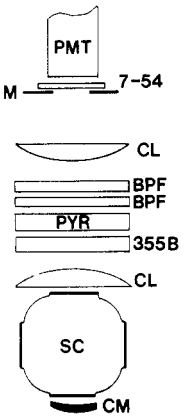

Figure 4. Detection optics and filter pack for PF–LIF HONO detection system: 7-54, colored glass filter; 355B, 355-nm blocking filter; BPF, band pass filter (309-nm); CL, fluorescence collection lens; CM, fluorescence collection mirror; M, PMT mask; PMT, photomultiplier tube; PYR, pyridine solution filter; SC, sampling chamber.

As illustrated in Figure 3, the main sampling line consisted of a 0.95-cm-i.d. black Teflon tubing, having an overall length of ~9 m. (Black tubing was selected over conventional translucent Teflon to eliminate the possibility of HONO photolysis within the sampling line by fluorescent lights used to illuminate the laboratory.) The ambient air intake for this system was located 3 m beyond a brick and mortar laboratory wall located on the eastern side of the Baker Research Building on the Georgia Tech campus. The inlet was ~10 m above ground level, and its location was such that it bordered a lightly traveled street on the Georgia Tech campus.

At two locations along the Teflon sampling line, 0.3 and 4.0 m from the inlet, were located Teflon "tee" assemblies that permitted injection of other gases (e.g., ozone/air or HONO/air) into the ambient air stream for calibration purposes.

The fluorescence chamber connected to the Teflon sampling line consisted of a 0.8-L all-quartz cell containing eight viewing ports. The entire sampling cell assembly was further enclosed in an all-metal chamber such that no room light entered the cell. The average residence time of HONO in the sampling system was 1.8 s, with a worst case time of ~2.5 s. Thus, using the results given in ref 16 and assuming a sticking coefficient of 1×10^{-6} [~12 times higher than that reported for HNO_3 by Grosjean (*24*)], the maximum HONO sampling line loss was estimated to be ~4% for the conditions employed in our system.

Fluorescence Detection System. The fluorescence detection optics and optical filter pack assembly, shown in Figure 4, are derivatives of an earlier system described in ref 25. They also are identical in their optical configuration with the system previously described in ref 16 and 26, except for the addition of a 355-nm chemical blocking filter [described by Bradshaw (*22*)].

Electronic Detection System. The detection electronics employed in the HONO detection system were similar to those used in other single-photon LIF systems by our group such as those previously discussed in ref 15, 25, and 26. The data collection system consisted of a small data-logging microcomputer (Creative Micro Systems, Inc., Model 9687), an interactive terminal, and a printer. This

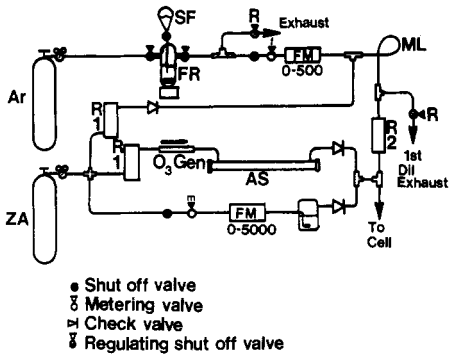

Figure 5. Schematic diagram of HONO flow calibration system: AR, argon cylinder; AS, absorption cell; FM, linear mass flowmeter; FR, HONO flow reactor; ML, mixing loop; R2, Teflon rotameter; SF, sodium nitrite solution; ZA, zero air.

system was essentially equivalent to the one previously described (*16*). It was used to collect and store information from both a gated-charge integrator and an array of other instruments that provided ancillary measurements of other atmospheric parameters.

Measurements Sequencing. The microcomputer system, previously mentioned in conjunction with our data-logging activities, was also employed in the HONO system for purposes of cycling the OH analysis laser through a timing sequence for collecting OH/HONO signal information. This cycle involved measurements both with and without the passage of the 355-nm photolysis beam through the sample cell and with the OH analysis beam "on" resonance with the OH $A^2\Sigma$–$X_2\pi$ transition (typically the Q_1^1 transition) as well as shifted to regions at both slightly higher and lower nonabsorbing wavelengths. Each of the above measurement events within a total measurement cycle consisted of 30-s integration time periods.

Flow Calibration System. Figure 5 shows a schematic diagram of the HONO PF–LIF flow calibration system. This system is of the dynamic dilution type and was designed to allow either HONO/air or O_3/H_2O/air mixtures to be introduced into the sampling chamber. The flow system was constructed entirely of glass, quartz, stainless steel, and Teflon, with small areas of contact with Viton O-rings and seals. Those portions of the system in contact with HONO gas mixtures consisted of Teflon, except for one stainless steel flowmeter and a small length of Pyrex glass used in the rotameters and the HONO generator.

Nitrous acid was produced by the method of Cox (*19, 20*) which involved the reaction of sodium nitrite with H_2SO_4 acid. This method produces HONO via the reaction of nitrite ion with H_3O^+. However, side reactions involving the nitrite ion and impurities also result in the simultaneous production of some NO_2. For the conditions used in this study, the ratio of HONO to NO_2 was typically found to lie between 1.5 and 2.0.

The HONO content from the first dilution stage was determined by near-ultraviolet absorption spectroscopy. This value, in combination with the final dilution factor, was used to calculate the HONO concentration in the sampling cell. With a two-stage dilution system, the HONO concentration levels achievable were 2 ppbv for ambient air calibrations and 10 ppbv for laboratory calibrations. With the addition of a third stage of dilution, HONO levels as low as 10 pptv were achieved in the sampling chamber.

The calibration system shown in Figure 5 could also be operated as an OH calibration system by using the O_3/H_2O calibration technique described by Rodgers et al. (*16*). In this system, known concentrations of hydroxyl radicals were produced by the UV photolysis of ozone [i.e., $O_3 + h\nu \rightarrow O(^1D) + O_2$, $O(^1D) + H_2O \rightarrow 2OH$].

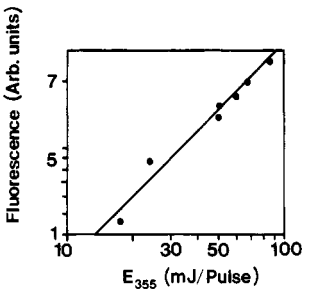

Figure 6. Photolysis laser energy scaling of PF–LIF HONO fluorescence signal (laboratory results)—nonforced least-squares fit of data.

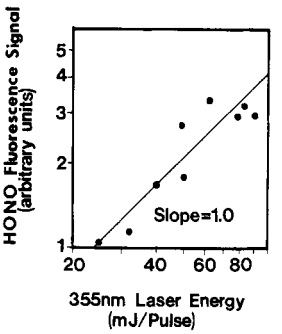

Figure 7. Photolysis laser energy scaling of PF–LIF HONO fluorescence (outside air measurements)—nonforced least-squares fit of data.

System Performance

Laser Null Experiments. To demonstrate that neither the OH analysis/probe laser tuning sequence nor the photolysis laser on/off sequencing resulted in the production of artifact OH/HONO signals, a series of laser null experiments were performed. In these tests the complete detection system, including the air sampling subsystem, was used to carry out a HONO measurement exercise except that in these experiments the OH analysis laser was tuned to a nearby spectral region devoid of OH absorption. In these tests, the signal from HO fluorescence should have been zero with statistically significant deviations from zero indicating the prescence of artifacts. To the limit of the experimental resolution (~1 part in 150), no system-generated artifacts were identified.

System Linearity Tests. While the laser null experiments provided evidence that system-generated artifacts were an insignificant component of the total signal, since these tests produced no signal, they still did not provide information on the expected accuracy of scaling the recovered fluorescence signal to standard conditions.

The linearity of the PF–LIF signal with 355-nm laser energy was demonstrated both for the case of laboratory mixtures of HONO in air, generated by the flow calibration system, and for measurements made with ambient air. Figure 6 shows the results of a laboratory 355-nm energy scaling test. This test was performed at relatively high concentrations of HONO (86 ppbv) and therefore shows a strong linear dependence of the fluorescence signal with 355-nm laser energy. On the other hand, fluorescence scaling experiments using outside air were more difficult due to changing atmospheric conditions, especially as related to the stability of the ambient level of HONO. Figure 7 shows the results of a 355-nm energy scaling tests performed on the night of 2/3/86. As can be seen from this plot, the much lower ambient concentration of HONO, together with the higher degree of variability in the level of HONO, resulted in noticeably higher scatter in these data than those recorded during the laboratory tests. Even so, the slope of the regression line indicates a linear de-

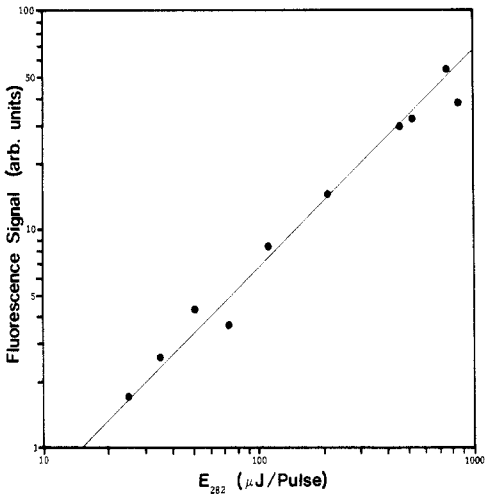

Figure 8. Probe laser energy scaling of PF–LIF HONO fluorescence signal (laboratory results)—nonforced least-squares fit of data.

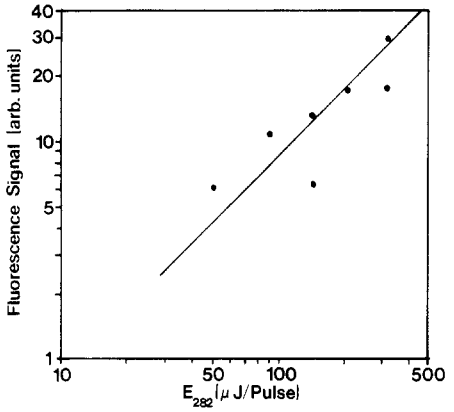

Figure 9. Probe laser energy scaling of PF–LIF HONO fluorescence (outside air measurements)—nonforced least-squares fit of data.

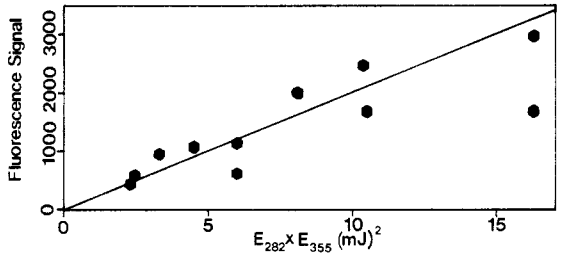

Figure 10. Photolysis/probe laser energy scaling of PF–LIF HONO signal (outside air measurements)—nonforced least-squares fit of data.

pendence of the PF–LIF fluorescence signal on 355-nm laser energy.

Figures 8 and 9 give the results of similar scaling tests performed with the energy of the 282-nm OH analysis laser beam. In this case, the laboratory test was performed at a somewhat reduced HONO concentration (22 ppbv) relative to the 355-nm test. By contrast, the ambient air 282-nm scaling test (conducted on 2/11/86) was conducted at higher concentrations of HONO (e.g., ~1.5 ppbv) than the 355-nm energy scaling tests ([HONO] ≃ 0.5 ppbv). In fact, at this higher HONO concentration level, it was possible to conduct tests where both the 355- and 282-nm energies were varied. The latter results are shown in Figure 10. All of these data (e.g., Figures 8–10) indicate that within the experimental error, the PF–LIF fluorescence signal was linearly dependent upon both the 355- and 282-nm energies.

Calibrations. A number of system calibrations, using both the O_3/H_2O and the HONO standard addition technique, were performed during the development of the

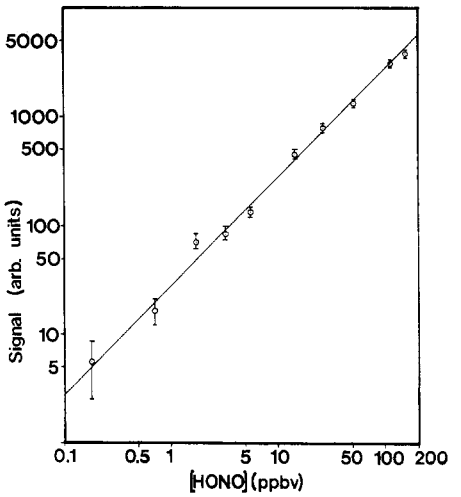

Figure 11. Calibration plot for PF–LIF HONO detection system (laboratory results)—nonforced least-squares fit of data.

Table I. Normalized Ambient Air System Calibration Numbers

date	HONO std addn	O_3/H_2O type calibrn
12/23/85[a]		1740[b]
12/24/85[a]	1603[c]	
1/18/86[a]	2002	
2/2/86		1909
2/3/86		2466
2/5/86	2970	2525
2/9/86		2145
2/11/86		1844
2/16/86	1953	
2/28/86	2116	
3/9/86	2306	
3/16/86		1699
3/20/86	2064	
3/21/86	2125	1936
3/23/86	2613	
3/29/86		2080
av	2195 ± 374 (1σ)	2038 ± 279 (1σ)

[a] These calibration numbers also required scaling for a change in optical filter pack transmission (–1.7×). [b] All O_3/H_2O calibration numbers are based on a value for E_1 of 0.048. [c] Units on calibration numbers are photons/300 laser shots per ppbv HONO at 100 mJ (355 nm) and 0.1 mJ (282 nm) under dry conditions.

HONO PF–LIF instrument. These calibration tests were designed to demonstrate the linear response of the PF–LIF technique to changes in HONO concentration. The results are shown in Figure 11. This figure demonstrates the linear response of the PF–LIF system over a HONO concentration range of 185 pptv–150 ppbv. The lower limit of 185 pptv was not a fundamental system limitation but rather the lowest concentration of HONO that could be reliably generated by the existing three-stage dynamic dilution system.

Ambient air calibrations were performed by both the O_3/H_2O and the HONO standard addition approaches. The results of these calibrations are given in Table I. In each case, the calibration numbers have been normalized to a set of "standard" conditions in order to facilitate comparison between the different measurements.

As can be seen from Table I, the good agreement between the two calibration approaches (agreement to within ~7%) can be taken as at least qualitative evidence that any systematic errors present in our calibration procedures were small.

A theoretical calculated calibration number based on equations given in ref 17 (2580 ± 50%) has been compared

Table II. HONO Sample Loss Tests

date	1/18/86	3/20/86
position 1 (0.3 m from inlet)	1861 ± 303 (2σ)[a]	2064 ● 103
position 2 (4 m from inlet)	2002 ± 245	2121 ± 109
position 3 (at sampling chamber)	2289 ● 277	1965 ± 144

[a] Calibration numbers in photons/300 laser shots per ppbv HONO at 100 mJ (355 nm) and 0.1 mJ (282 nm) under dry conditions. The ambient HONO level on 1/18/86 was ≤ 200 pptv and that on 3/20/86 was 2.2 ppbv. The injected level of HONO on 1/18/86 was 6.4 ppbv and that on 3/20/86 was 5.5 ppbv.

to those experimentally derived from the HONO standard addition tests (e.g., 2195 ± 374) and from the O_3/H_2O calibration method (e.g., 2038 ± 279). In this comparison, we find that the experimentally derived values are ~20% lower than the theoretical estimate; however, considering the combined uncertainties of the theoretical estimate and the experimental measurements, this level of agreement would appear to be excellent.

Interference and Sample Loss Tests. As mentioned previously, two of the most important considerations in testing any in situ type of detection system are establishing that the system is free from interferences and that sampling losses are equally insignificant. In this regard, the results of the tests described above place upper limits on certain types of interferences. For example, the observation that the fluorescence signal was linear in both 355- and 282-nm laser energy precludes any significant contribution from two-photon processes, including the O_3/H_2O interference discussed in Appendix A. Additionally, the data collection scheme employed served to eliminate the presence of any OH interference arising from secondary chemistry involving the probe laser beam. Thus, considering the high spectroscopic selectivity of the laser-induced fluorescence approach, the only other potential interference that required exploration involved the possible generation of OH by the 355-nm photolysis beam, through either direct photolysis or secondary chemistry. However, a careful examination of the most likely possibilities (e.g., H_2O_2, HNO_3, and CH_3OOH) has shown that direct photolysis of these species would have a negligibly small impact.

Likewise, the probability of interference due to secondary chemistry involving the 355-nm beam during the very short time delay (~12 ns) between the passage of the photolysis beam and the OH analysis/probe laser beam would appear to be quite low. However, this would not necessarily be true if the chemistry occurred in the 100-ms interval between two sequential 355-nm laser pulses. In fact, experiments were undertaken to check for OH production arising during the time period between laser pulses. These tests involved injection of small quantities of OH scavenging propylene (~150 ppbv) into the sample gas stream just before it entered the sampling chamber. What was observed in these experiments was that the PF–LIF signals made both with and without the propylene injection did not differ within their standard errors.

Sample losses of HONO, the second major area of concern, were evaluated on two occasions as part of our HONO standard addition calibrations. The results of these tests are summarized in Table II.

The 1/18/86 measurements were made under worst case conditions of misty rain and near 100% relative humidity, while the 3/20/86 measurements were made under clear conditions. These tests suggest that, in agreement with the theoretical estimates given earlier, HONO sampling line losses are insignificant in our system when HONO levels are in the low ppbv range.

Field Measurements. To demonstrate the utility of the PF–LIF system for the detection of HONO, measurements were performed on 27 evenings between mid-December 1985 and the end of March 1986 in Atlanta, GA. The results from these experiments have been submitted for publication (27). In brief, during this measurement period concentrations of HONO were observed to range from below the instrumental limit of detection (normally in the few tens of parts per trillion) to as high as 6.4 ppbv. Typical peak nighttime concentrations were in the low ppbv range.

Summary

A new in situ laser-based detection system for measuring atmospheric HONO has been tested. This system has proven to be both highly sensitive and specific for the detection of HONO. The system has been calibrated by using two different approaches: one based on standard addition of HONO and the second based on a previously developed OH calibration procedure. Both approaches were shown to be in good agreement with theory. Sampling losses were evaluated both theoretically and experimentally and were found to be insignificant.

This newly developed photofragmentation/laser-induced fluorescence system was found to have a detection limit in the low tens of parts per trillion for typical integration times of 15 min in duration. This sensitivity is roughly equivalent to that achieved by the long-path absorption technique. Future improvements in the PF–LIF system, such as increasing the fluorescence detection efficiency, are expected to lower the detection limit to HONO levels of less than 10 pptv.

Appendix A

Evaluation of O_3/H_2O Interference to the PF–LIF Detection of HONO. A measurement of ambient atmospheric OH by single-photon laser-induced fluorescence detection is subject to interference due to OH produced by the laser photolysis of atmospheric ozone. The reaction sequence is given by

$$O_3 + h\nu \rightarrow O(^1D) + O_2(^1\Delta) \quad \text{(A1)}$$

$$O(^1D) + M \rightarrow O(^3P) + M \quad \text{(A2)}$$

$$O(^1D) + H_2O \rightarrow 2OH \quad \text{(A3)}$$

The signal arising from the O_3/H_2O interference has been evaluated previously; see ref 16 and 28.

As related to the detection of HONO, to a first approximation the fractional interference in the measurement of HONO can be defined in terms of the signal ratio:

$$\frac{S_{\text{interf}}}{S_{\text{OH(HONO)}}} = (4.9 \times 10^{-4} E_2\ (\text{mJ/pulse}) \times [O_3(\text{ppbv})] \times [H_2O(\text{Torr})])/[\text{HONO(ppbv)}] \quad \text{(A4)}$$

where E_2 is the energy of the 282-nm laser for a beam cross-sectional area of 0.8 cm^2. By use of eq A-4 under typical atmospheric conditions with [HONO] = 1 ppbv, a 282-nm laser energy of 0.1 mJ/laser shot and an $[O_3][H_2O]$ product of 300 ppbv Torr, the calculated fractional interference is found to be ~1.5%.

Registry No. OH, 3352-57-6; HONO, 7782-77-6.

Literature Cited

(1) Leighton, P. A. *Photochemistry of Air Pollution*; Academic: New York, 1961.

(2) Demerjian, K. L.; Kerr, J. A.; Calvert, J. G. *Advances in Environmental Science and Technology*; Pitts, J. N., Jr.,

Metcalf, R. L., Eds.; Wiley: New York, 1974; Vol. 4.
(3) Finlayson, B. J.; Pitts, J. N., Jr. *Science (Washington, D.C.)* **1976**, *192*, 111-119.
(4) Stockwell, W. R.; Calvert, J. G. *J. Geophys. Res., C: Oceans Atmos.* **1983**, *88*, 6673-6682.
(5) Platt, U.; Perner, D.; Harris, G. W.; Winer, A. M.; Pitts, J. N., Jr. *Nature (London)* **1980**, *285*, 312-314.
(6) Harrison, G. W.; Carter, W. P. L.; Winer, A. M.; Pitts, J. N., Jr.; Platt, U.; Perner, D. *Environ. Sci. Technol.* **1982**, *16*, 414-419.
(7) Nash, T. *Tellus* **1974**, *26*, 176-180.
(8) Ferm, M.; Sjödin, A. *Atmos. Environ.* **1985**, *19*, 979-985.
(9) Penkett, S. A.; Sandalls, F. J.; Jones, B. M. R. *VDI-Ber.* **1977**, *No. 270*, 47-54.
(10) Sjödin, A.; Ferm, M. *Atmos. Environ.* **1985**, *19*, 985-992.
(11) Perner, D.; Platt, U. *Geophys. Res. Lett.* **1979**, *6*, 917-920.
(12) Platt, U.; Perner, D. *J. Geophys. Res., C: Oceans Atmos.* **1980**, *85*, 7453-7458.
(13) Harris, G. W.; Winer, A. M.; Pitts, J. N.; Platt, U.; Perner, D. *Springer Ser. Opt. Sci.* **1983**, *39*, 106-113.
(14) Rodgers, M. O.; Asai, K.; Davis, D. D. *Appl. Opt.* **1980**, *19*, 3597.
(15) Rodgers, M. O.; Davis, D. D. XVII Informal Conference on Photochemistry; Boulder, CO, June 1986.
(16) Rodgers, M. O.; Bradshaw, J.; Sandhold, S. T.; KeSheng, S.; Davis, D. D. *J. Geophys. Res., C: Oceans Atmos.* **1985**, *90*, 12819-12834.
(17) Rodgers, M. O. Ph.D. Dissertation, Georgia Institute of Technology; Atlanta, GA, 1986.
(18) King, G. W.; Moule, D. *Can. J. Chem.* **1962**, *40*, 2057-2065.
(19) Cox, R. A. *J. Photochem.* **1974**, *3*, 291-304.
(20) Cox, R. A. *J. Photochem.* **1974**, *3*, 175-188.
(21) Davis, D. D.; Bradshaw, J. D.; Sandholm, S. T. *Annual Report to the Coordinating Research Council*; Georgia Institute of Technology: Atlanta, GA, August, 1985.
(22) Bradshaw, J. D.; Rodgers, M. O.; Davis, D. D. *Appl. Opt.* **1984**, *23*, 2134-2145.
(23) Vasudev, R.; Zare, R. N.; Dixon, R. N. *Chem. Phys. Lett.* **1983**, *96*, 399-402.
(24) Grosjean, D. *Environ. Sci. Technol.* **1985**, *19*, 1059-1065.
(25) Bradshaw, J. D.; Rodgers, M. O.; Davis, D. D. *Appl. Opt.* **1982**, *21*, 2493-2500.
(26) Davis, D. D.; Heaps, W. S.; Philen, D.; Rodgers, M.; McGee, T.; Nelson, A.; Moriarty, A. J. *Rev. Sci. Instrum.* **1979**, *50*, 1505-1516.
(27) Rodgers, M. O.; Davis, D. D., submitted for publication in *Environ. Sci. Technol.*
(28) Davis, D. D.; Rodgers, M. O.; Fischer, S. D. *Geophys. Res. Lett.* **1981**, *8*, 73-76.

Received for review September 14, 1987. Accepted June 13, 1988. We acknowledge the support of this research by the Coordinating Research Council, Inc., under contract CAPA-19-80(3-83).

A Quiet Sampler for the Collection of Semivolatile Organic Pollutants in Indoor Air

Nancy K. Wilson*

Atmospheric Research and Exposure Assessment Laboratory, U.S. Environmental Protection Agency, Research Triangle Park, North Carolina 27711

Michael R. Kuhlman, Jane C. Chuang, and Gregory A. Mack

Battelle Columbus Division, Columbus, Ohio 43201

James E. Howes, Jr.

Combustion Engineering—Environmental, Incorporated, Chapel Hill, North Carolina 27514

■ A prototype air sampler that is quiet and transportable was designed and constructed for the collection of semivolatile organic compounds in indoor air. The sampler combines a filter and adsorbent in series and can be operated at a flow rate sufficient to collect enough organic matter for chemical analysis and microbioassay. The acoustic insulation of the sampler allows it to meet a noise criterion of NC-35, roughly the sound level in a quiet conference room. Operation of the sampler with its exhaust both vented and not vented showed that the sampler itself does not significantly affect the levels of polynuclear aromatic hydrocarbons in indoor air. Therefore it is unnecessary to vent the sampler outdoors during indoor air sampling for these compounds, thus minimizing the effect of the sampler on the house air exchange rate.

Introduction

Several studies (*1-9*) have shown that many polynuclear aromatic hydrocarbons (PAHs) and nitrated PAHs found in air are carcinogens, mutagens, or both. The analytical methodology to determine these compounds is established. However, methodology for sampling semivolatile organic compounds [those with vapor pressures roughly 10^{-2}–10^{-8} kPa (10^{-1}–10^{-7} Torr)] in indoor air is not equally established. Devices currently used in air sampling to collect adequate material for chemical analysis and bioassay (*10, 11*) are not suitable for air sampling in homes because of their size, noise, and lack of portability. In a previous indoor air study (*2, 8, 9*), we put the sampler pump outside the house in an insulated enclosure to minimize the noise level. We made different modifications, which depended on the structure of each house sampled, to allow connection of the sampling module to the pump by passing the connecting tube through a window port. These modifications of the sampling system increased the difficulty in sampling and the inconvenience experienced by the residents. We have therefore developed an indoor air sampler that is quiet, transportable, and reasonably unobtrusive and that can be located entirely inside the house during sampling.

Besides the physical requirements mentioned above, a principal requirement for the indoor sampler described here is that it collect quantities of particles and vapors sufficient for both chemical analysis and microbioassay. Another requirement is that it collect the sample in a time short enough that an individual's time profile of exposure to the compounds of interest can be defined. We examined available data on the typical concentrations of PAHs and other compounds of interest in indoor air and estimated the mass required to analyze the target compounds accu-

 0013-936X/89/0923-1112$01.50/0